Tectonophysics xxx (2014) xxx–xxx

Contents lists available at ScienceDirect

Tectonophysics

journal homepage: www.elsevier.com/locate/tecto

The 2012 Emilia seismic sequence (Northern Italy): Imaging the thrust fault system by accurate aftershock location

Aladino Govoni [a,b,*], Alessandro Marchetti [a], Pasquale De Gori [a], Massimo Di Bona [a], Francesco Pio Lucente [a], Luigi Improta [a], Claudio Chiarabba [a], Anna Nardi [a], Lucia Margheriti [a], Nicola Piana Agostinetti [c], Rita Di Giovambattista [a], Diana Latorre [a], Mario Anselmi [a], Maria Grazia Ciaccio [a], Milena Moretti [a], Corrado Castellano [a], Davide Piccinini [a]

[a] INGV — Istituto Nazionale di Geofisica e Vulcanologia, Via di Vigna Murata 605, 00143 Rome, Italy
[b] OGS — Istituto Nazionale di Oceanografia e Geofisica Sperimentale, Via Treviso, 55, 33100 Udine, Italy
[c] Dublin Institute for Advanced Studies, 10 Burlington Road, Dublin 4, Ireland

ARTICLE INFO

Article history:
Received 26 June 2013
Received in revised form 20 February 2014
Accepted 23 February 2014
Available online xxxx

Keywords:
Seismology
Hypocentral location
Seismic sequence
Velocity model
Thrust fault system
Po alluvial Plain

ABSTRACT

Starting from late May 2012, the Emilia region (Northern Italy) was severely shaken by an intense seismic sequence, originated from a M_L 5.9 earthquake on May 20th, at a hypocentral depth of 6.3 km, with thrust-type focal mechanism. In the following days, the seismic rate remained high, counting 50 $M_L \geq 2.0$ earthquakes a day, on average. Seismicity spreads along a 30 km east–west elongated area, in the Po river alluvial plain, in the nearby of the cities Ferrara and Modena. Nine days after the first shock, another destructive thrust-type earthquake (M_L 5.8) hit the area to the west, causing further damage and fatalities. Aftershocks following this second destructive event extended along the same east-westerly trend for further 20 km to the west, thus illuminating an area of about 50 km in length, on the whole. After the first shock struck, on May 20th, a dense network of temporary seismic stations, in addition to the permanent ones, was deployed in the meizoseismal area, leading to a sensible improvement of the earthquake monitoring capability there. A combined dataset, including three-component seismic waveforms recorded by both permanent and temporary stations, has been analyzed in order to obtain an appropriate 1-D velocity model for earthquake location in the study area. Here we describe the main seismological characteristics of this seismic sequence and, relying on refined earthquakes location, we make inferences on the geometry of the thrust system responsible for the two strongest shocks.

1. Introduction

In May–June 2012, Emilia seismic sequence affected a 50-km wide, roughly E–W trending region located at the southern edge of the Po river alluvial plain (Fig. 1). The sequence started on May 20 (02:03:53 UTC), with a M_L 5.9 (M_W 5.9) earthquake, preceded by a M_L 4.1 foreshock, 3 h earlier (Scognamiglio et al., 2012). This major event produced serious damages and five victims. The region was then shaken by thousands of earthquakes, six of them with $M_L \geq 5.0$ (see Table 1). Among these, a M_L 5.8 earthquake (M_W 5.7), on May 29 (07:00:03 UTC), caused possibly more damages than the first shock, bringing the death toll to the official number of seventeen (ten more, among the 350 injured, will die in the following days) and completely destroyed buildings and structures that were already affected by the 20th May earthquake (Tertulliani et al., 2012). Extensive liquefaction phenomena were triggered by the strongest events (Emergeo Working Group, 2013; Papathanassiou et al., 2012).

The Emilia seismic sequence took place in a relatively low seismic hazard area (Seismic Hazard Map of Italy MPS04 from MPS Working Group (2004)), where no large historical earthquakes are reported, the largest one being the November 17, 1570, M_W 5.5 Ferrara event located to the east of the sequence (Fig. 1a; data source Parametric Catalogue of Italian Earthquakes, CPTI11 after Rovida et al. (2011)). At the same time, this is one of the most densely populated areas in Italy, which is part of the major agricultural and industrial district of the country. Moreover, the thick cover of young, unconsolidated sediments in the Po alluvial plain (Fig. 1b) strongly amplifies the seismic shaking (Bordoni et al., 2012; Margheriti et al., 2000; Marzorati and Bindi, 2006), and even moderate earthquakes can have catastrophic effects.

In this study we analyze the first month of the aftershock sequence, until June 20th, using data from permanent and temporary seismic stations (Moretti et al., 2012). Accurate earthquake locations allow us to define the space–time evolution of the seismicity, image the

* Corresponding author at: Istituto Nazionale di Geofisica e Vulcanologia - INGV Via di Vigna Murata, 605-00143 ROMA Italy.

http://dx.doi.org/10.1016/j.tecto.2014.02.013
0040-1951/

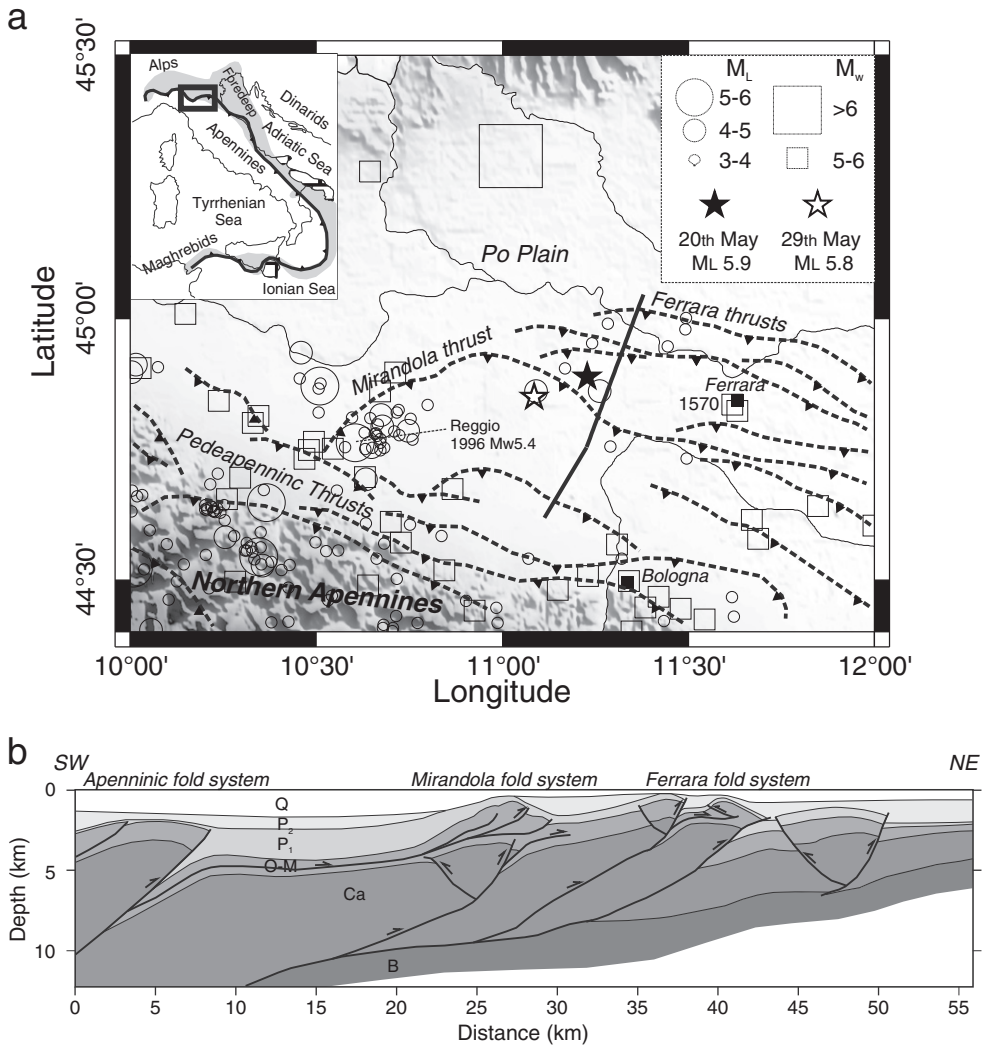

Fig. 1. (a) Simplified structural map of the Emilia region showing Northern Apennines main thrusts and the two mainshocks of the Emilia sequence, indicated by black (20 May, M_L 5.9) and white stars (29 May, M_L 5.8), respectively. Historical earthquakes from CPTI catalog (open squares; data source: Parametric Catalogue of Italian Earthquakes, CPTI11 after Rovida et al. (2011)) and instrumental seismicity between 1981 and 2012 (circles), are also shown. Solid square indicates the Ferrara town. Instrumental data are from CSI catalog (Castello et al., 2006) and ISIDe database (ISIDe Working Group, 2010). Thrust geometries are taken from Boccaletti et al. (2011). Dashed lines denote blind thrusts. The inset map shows a geologic sketch of Italy and location of the study region (black box). On this inset map the thick black line approximately indicates the Africa–Eurasia plate boundary. (b) Geological cross section along the black trace in panel a (modified after Carminati et al. (2010)): Q — continental and marine Quaternary deposits, P_2 — marine terrigenous deposits (upper-middle Pliocene), P_1 — evaporitic and terrigenous deposits (late Miocene–lower Pliocene), O–M — marly calcareous and terrigeneous deposits (Oligocene–Miocene), Ca — shallow to deep-water carbonates (Mesozoic–Eocene), B — Paleozoic basement.

geometry of the activated faults, improve the earthquake magnitude estimation, and give a seismotectonic interpretation, thus providing precious information useful as a basis for further specific studies.

2. Geological and seismotectonic setting

The Emilia sequence hit the central, roughly E–W trending, sector of the Ferrara arc belonging to the external fold-and-thrust system of the Northern Apennines belt (Fig. 1a). This NE-verging belt developed during Neogene and Quaternary in the framework of the collision between the European continental margin and the Adria microplate (Reutter et al., 1980). The fold-and-thrust system is completely buried by thick Quaternary sediments of the Po plain (Fig. 1b) and, consequently, has been defined principally by hydrocarbon exploration data. It consists of S-dipping blind thrusts and related folds, which involve a sedimentary succession mainly consisting of Triassic evaporites, Mesozoic–Early Tertiary shallow to deep-water carbonates, and Oligocene–Miocene clastic successions (Fig. 1b) (Carminati et al., 2010; Fantoni and Franciosi, 2010). Mesozoic units rest on Permo-Triassic clastic deposits and on the Paleozoic crystalline basement. Miocene strata are covered by syntectonic Plio-Pleistocene terrigenous deposits (mainly turbidites and marine sands) and Late Quaternary fluvio-lacustrine deposits. Thickness of the Plio-Quaternary cover is extremely variable and was controlled by the growth of thrust-propagation folds: it ranges from 7000 to 8000 m at the core of deepest synclines to about only 150 m at the top of thrust-related anticlines (Fig. 1b) (Margheriti et al., 2000).

In the aftershock region, the Ferrara arc is structured in two major fold-and-thrust systems: the Ferrara system in the northeast and the Mirandola system located in a more internal position in the southwest (Fig. 1a). The former includes WNW–ESE trending structures, the latter is strongly bent and changes in strike from W–E to NW–SE, moving from W to E. Both systems also include distinct and minor thrust splays, back-thrusts and related folds (Fig. 1b). While the shallow architecture of fold-and-thrust structures is well imaged in seismic reflection profiles down to about 5–7 km depth, the deep geometry of the thrust planes is poorly defined because data quality and reflectivity strongly deteriorate at depth. This drawback is particularly evident in the footwall side of major thrusts where lithological contrasts disappear. As a consequence,

Please cite this article as: Govoni, A., et al., The 2012 Emilia seismic sequence (Northern Italy): Imaging the thrust fault system by accurate aftershock location, Tectonophysics (2014), http://dx.doi.org/10.1016/j.tecto.2014.02.013

Table 1
Origin time, location and local magnitude (M_L) from this study of the largest events of the 2012 Emilia seismic sequence, with $M_L \geq 5.0$. (1) Moment magnitude (M_W), beach balls and focal plane parameters are from Scognamiglio et al. (2012), also on http://cnt.rm.ingv.it/tdmt.html.

Origin date time (UTC)	Latitude	Longitude	Depth	M_L	M_W (1)	Focal mechanism (1)	Strike1 Dip1 Rake1 Strike2 Dip2 Rake2 (1)
2012-05-20[a] 02:03:52.000	44.890	11.230	6.30	5.90	5.86		103; 46; 92 280; 44; 88
2012-05-20[a] 03:01:56.950	44.865	11.261	4.36	5.12	[b]	[b]	[b]
2012-05-20[a] 03:02:49.080	44.861	11.111	3.82	5.20	4.85		279; 64; 95 88; 27; 81
2012-05-20 13:18:02.000	44.813	11.441	3.35	5.25	4.96		291; 49; 90 111; 41; 90
2012-05-29 07:00:03.000	44.842	11.066	8.07	5.77	5.66		275; 52; 90 95; 38; 90
2012-05-29 11:00:25.000	44.856	10.941	8.68	5.03	[b]	[b]	[b]
2012-06-03 19:20:43.000	44.886	10.950	8.66	5.14	4.76		271; 71; 93 81; 20; 81

[a] Three of the largest events occurred before the temporary seismic network started operating, therefore for them the ISIDe database location is reported (data source: ISIDe).
[b] Two of the largest events were closely preceded or followed by other earthquakes that hindered the inversion for the TDMT calculation, therefore no focal parameters are available for them.

tectonic models of the Ferrara arc published in recent years present different interpretations of deep thrust structures. In particular, the outer thrusts are defined as high-angle faults deeply rooted in the basement (Picotti and Pazzaglia, 2008) or, alternatively, as flatting faults connecting down with a main low-angle basal detachment at the base of the Mesozoic succession (Boccaletti et al., 2011; Carminati et al., 2010).

Even though earthquake catalogs show that seismicity – both historical and instrumental – in the Emilia sequence area is low ($M_L < 5.0$) and sparse (Castello et al., 2006) (Fig. 1a), active shortening in the southern Po plain is well documented by anomalies in the hydrographic pattern (Burrato et al., 2003), folded Late Pleistocene strata in seismic profiles (Boccaletti et al., 2011) and GPS data (Serpelloni et al., 2005). Borehole breakouts (Montone et al., 2012) and CMT solutions (Pondrelli et al., 2006) indicate NE–SW regional shortening, with maximum horizontal stress (SH_{max}) directions generally perpendicular to the thrust fronts and to the axis of anticlines. In accordance, focal solutions of mainshocks and strongest aftershocks show prevalently thrust mechanisms (Malagnini et al., 2012a; Pondrelli et al., 2012; Scognamiglio et al., 2012).

3. Data analysis

For the number of reasons mentioned above – low historical seismicity, high industry and population density, alluvial nature of soils – the area affected by the seismic sequence is not among the most densely instrumented area in Italy (data source: Italian Seismological Instrumental and parametric Data-base, ISIDe by ISIDe Working Group, 2010). Thus, for the analysis we heavily rely on the data provided by several temporary seismic stations installed in the meizoseismal area soon after the sequence started (Fig. 2), many of which contributed to the real-time monitoring (Moretti et al., 2012). Until the end of June, more than 2000 aftershocks were detected by the Istituto Nazionale di Geofisica e Vulcanologia (INGV) earthquake monitoring system. Earthquakes were located by seismologists on seismic surveillance duty with the HYPOINVERSE-2000 code (Klein, 2002) using a 1D velocity model with two layers at 0–11-km (Vp = 5.0 km/s) and 11–38 km (Vp = 6.5 km/s) depth over a halfspace at depth >38 km with Vp = 8.0 km/s. These locations available in real time on the ISIDe website were used to obtain the first published results on the sequence (Scognamiglio et al., 2012; Ventura and Di Giovambattista, 2013).

For this study, all these earthquakes were carefully reprocessed providing accurate picks of P- and S-phases on the three-component digital recordings of stations within 120 km from the May 20th mainshock.

We also analyzed waveforms from further 1500 triggers, not detected as seismic events, in order to fill the gaps in the catalog due either to under-reporting of earthquakes that occurred in the coda of larger events (Enescu et al., 2007), or to the quasi-simultaneous occurrence of two or more earthquakes. We thus retrieve about 700 additional earthquakes, raising the initial set to 2712 earthquakes for a total of about 43,500 P- and 28,000 S-wave arrivals at 49 seismic stations.

4. 1-D velocity model

Great care has been taken in building the “ad hoc” 1-D model for earthquake relocation. As first step we located all the aftershocks using the program Hypoellipse (Lahr, 1989). The starting Vp model was taken from Malagnini et al. (2012a) who defined a shallow velocity profile gathering information from geological studies and seismic profiles. The average Vp/Vs for the studied crustal volume was computed using the modified Wadati method (Chatelain, 1978). In order to get a better Vp/Vs estimation for the crustal volume, where the bulk of seismicity developed, we used only observations of up-going ray-paths, thus discarding rays that traveled in the lower crust. We obtained a Vp/Vs of 1.90 (Fig. 3).

In order to compute the final 1-D model we apply the inversion scheme introduced by Kissling et al. (1994) and implemented in the code VELEST to an optimal sample of seismicity, representative of the seismogenic volume. For this exercise we only consider earthquakes that occurred after the temporary seismic network started operating. In order to have a homogeneous sampling of the entire seismogenic volume, this was partitioned into 4-km cubic cells and

Please cite this article as: Govoni, A., et al., The 2012 Emilia seismic sequence (Northern Italy): Imaging the thrust fault system by accurate aftershock location, Tectonophysics (2014), http://dx.doi.org/10.1016/j.tecto.2014.02.013

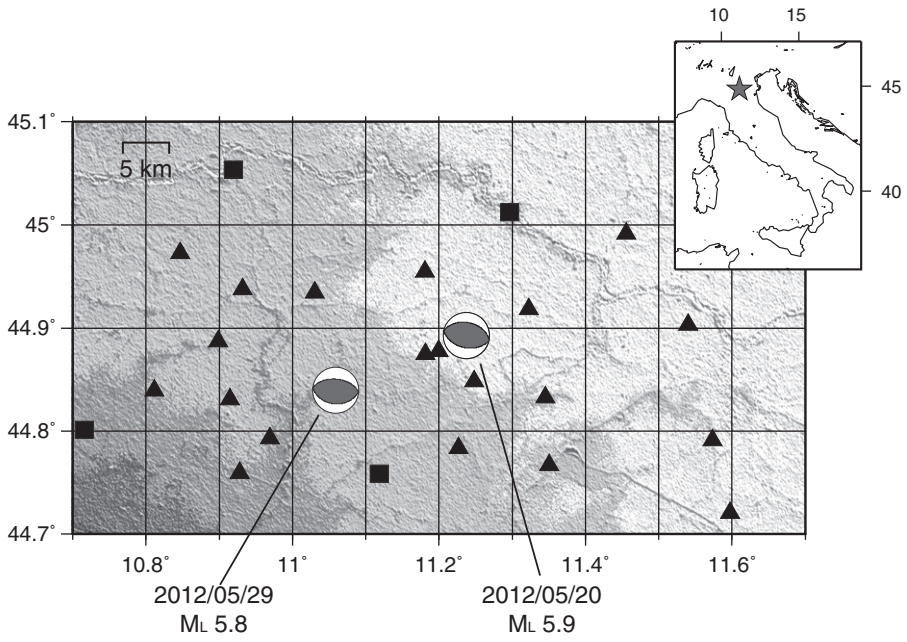

Fig. 2. Location of the INGV seismic stations operating in the meizoseismal area during the 2012 Emilia seismic sequence: black squares are the permanent stations belonging to the National Seismic Network; black triangles are the temporary seismic stations deployed soon after the 20th May earthquake struck. On the map, the focal mechanisms of the two mainshocks are also reported (Scognamiglio et al., 2012), indicating the epicenter of the 20th (M_L 5.9) and 29th (M_L 5.8) May earthquakes, respectively. The background of the map is a topographic model of Italy with 90 m resolution grid. The dark gray star on the inset map of Italy indicates the location of the meizoseismal area.

for each cell no more than 10 events with location errors lower than 1 km, rms < 0.5 s, and at least 10 P- and 5 S-wave readings, were selected. We obtained a representative subset of 808 aftershocks for the subsequent inversion. We then inverted P- and S-wave arrival times of this subset of events to simultaneously compute hypocenter solutions and the best 1-D Vp and Vs model. The input velocity model for VELEST is parameterized by horizontal layers with Vp and Vp/Vs values varying with depth, according to the adopted starting model (Malagnini et al., 2012a). The damping parameter was chosen by running different inversions as the best trade-off between data variance reduction and model complexity. The optimum model (Fig. 4) was achieved after 10 iterations, achieving a final rms of 0.17 s with a variance reduction of 52%. The model solution includes the station corrections that account for the along-path velocity heterogeneities not adequately modeled by the laterally homogeneous 1-D velocity structure. In its first layer, down to 4 km depth, the obtained 1-D model (Fig. 4) features low P-wave velocity of 3.3 km/s, accompanied by very high Vp/Vs ratio of about 2.1, resulting into a S-wave velocity of about 1.6 km/s. These are values typical for sedimentary covers made up of soft, unconsolidated sediments (e.g. Artemieva, 2002), and are consistent with the presence in the Po plain of thick Plio-Quaternary successions mainly formed by saturated sandy deposits (Fig. 1b). Below this first layer, both the P-wave velocity and Vp/Vs ratio profiles display values characteristic for consolidated sedimentary rocks like Mesozoic evaporites and carbonates, which, as in our case, are the typical seismogenic rock in the Italian Apennines (Ciccotti and Mulargia, 2004; Trippetta et al., 2013). The relatively high Vp/Vs values (1.8 — 1.9) down to 12 km depth can be related to fractured and fluid saturated Mesozoic carbonates (Chiarabba et al., 2009; Valoroso et al., 2011).

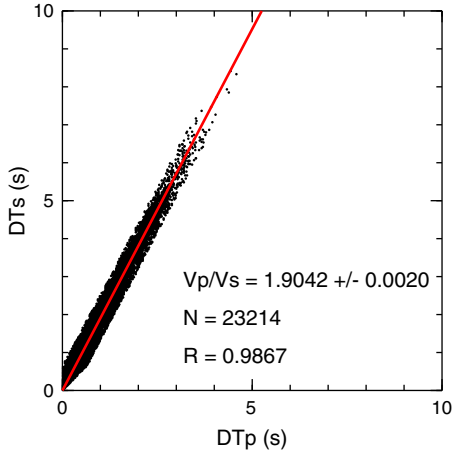

Fig. 3. Wadati (1933) diagram computed on all the earthquakes with up-going ray-paths to the stations. For each event, DTp and DTs are the differences between P- and S-phase arrival times, respectively, at couples of stations. N is the number of measurements. The Vp/Vs value is the slope of the straight line, while R is the correlation coefficient of the linear regression.

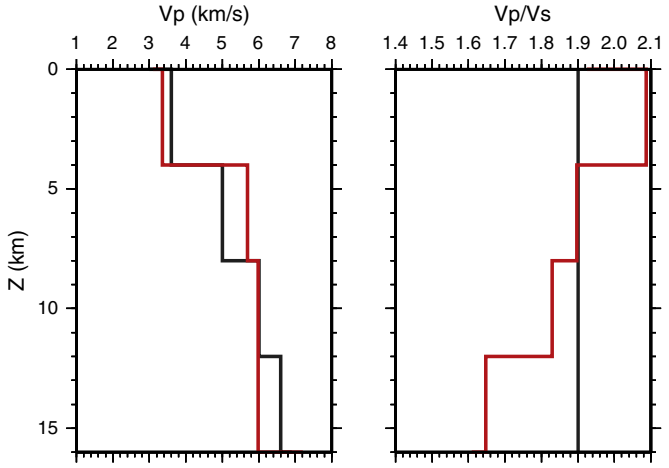

Fig. 4. Starting (dark gray) and final (red) P-wave 1-D velocity model (left panel) and Vp/Vs (right panel) computed using the VELEST code (Kissling et al., 1994). (For interpretation of the references to color in this figure legend, the reader is referred to the web version of this article.)

Please cite this article as: Govoni, A., et al., The 2012 Emilia seismic sequence (Northern Italy): Imaging the thrust fault system by accurate aftershock location, Tectonophysics (2014), http://dx.doi.org/10.1016/j.tecto.2014.02.013

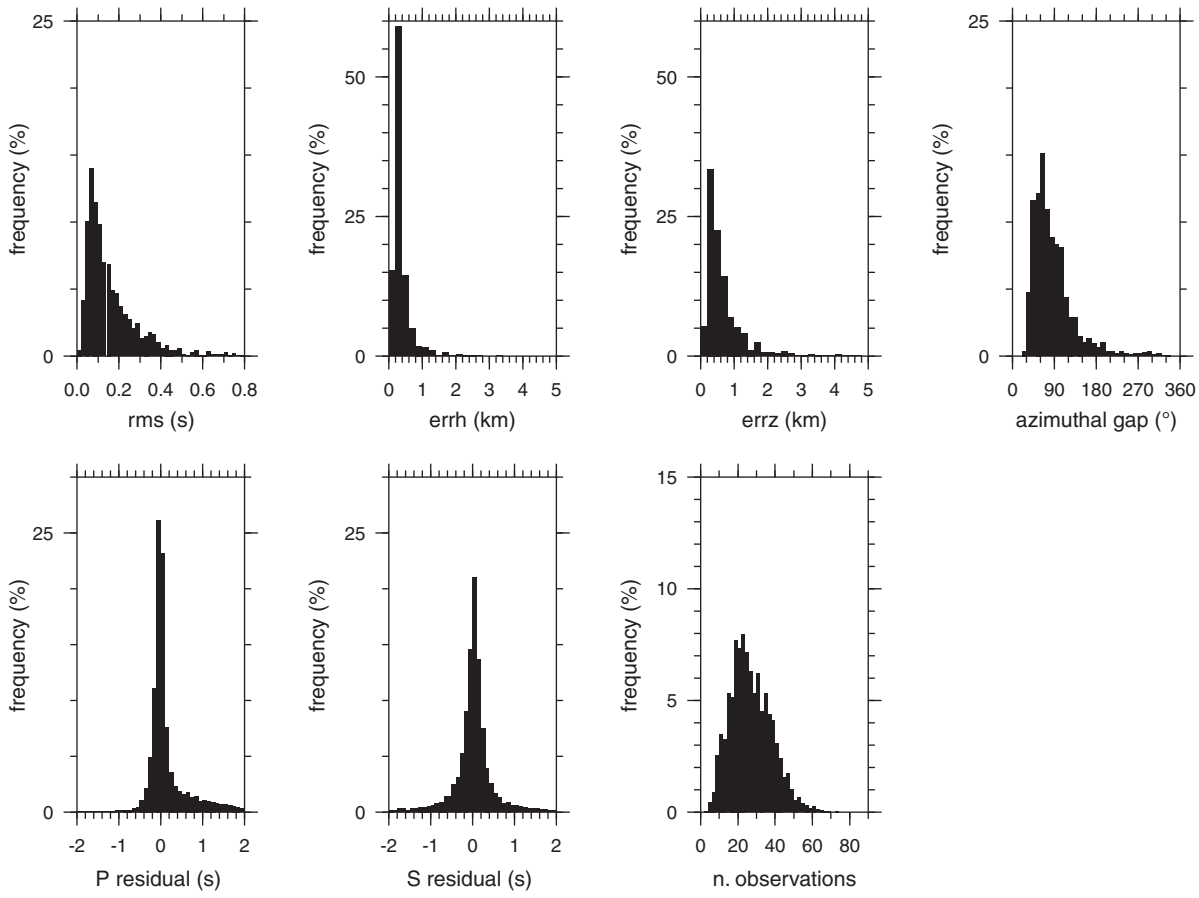

Fig. 5. Histograms summarizing the main outputs of the localization procedure, in terms of frequency of observations for each of the following parameters (from top left to bottom right): residual rms (s); horizontal location errors (km); vertical location errors (km); azimuthal gap between stations (°); P-phase residuals (s); S-phase residuals (s); number of observations.

Finally, we use this best 1-D Vp and Vs model – plus station corrections – to relocate the whole set of aftershocks through the Hypoellipse code (Lahr, 1989). We obtain a final set of 1745 well located earthquakes, with location errors lower than 1 km, rms < 1 s, maximum azimuthal gap between stations of 180°, and at least 7 P- and S-wave readings. We note that, P- and S-velocities in our 1-D model are, on average, much slower than those in the model used to obtain the locations available on the ISIDe website (see the above section), thus resulting into shallower hypocenters if compared to the first published results on the sequence (Ventura and Di Giovambattista, 2013). The performances of the adopted approach, in terms of rms, error magnitude and residual distribution can be evaluated in Fig. 5, where some of the main outputs of the localization procedure are summarized.

5. The relocated earthquake catalog

Results of the analysis described above are summarized in Fig. 6, where map and cross section views of the seismic sequence are provided. In Fig. 6, the vertical cross section AA' is drawn roughly parallel to the average strike of the two mainshock ruptured planes (103° and 95°, respectively, for the 20th and the 29th May events), inferred from the time-domain moment tensor solutions (TDMT) (Scognamiglio et al., 2012; see also http://cnt.rm.ingv.it/tdmt.html); the vertical cross sections going from BB' to II' are drawn roughly perpendicular to this average strike. Also, we project the earthquakes located within 1.5 km distance from the vertical plane on the cross ections going from BB' to II', while on the cross section AA' the whole set of analyzed earthquakes is projected. The cross sections DD' and FF' are drawn across the 29th and 20th May mainshocks, respectively.

The relocated earthquake catalog represents a sensible improvement on the existing one (e.g. Scognamiglio et al., 2012; Ventura and Di Giovambattista, 2013) in terms of geometrical definition of the activated fault system, whose characteristics are here more clearly recognizable. This relocated catalog is available in Appendix A, as supplementary data (kml format), and is going to be integrated in the Italian Seismic Bulletin released by INGV (http://bollettinosismico.rm.ingv.it/).

A major shortcoming is that, being the used Vp and Vs model the optimal 1-D approximation of the velocity structure in the seismogenic volume, it works well only when most of the seismic rays are within this volume, i.e. when most of the seismic stations are above the focal region. This condition is achieved when temporary seismic network started operating, about 8 hours after the May 20th M_L 5.9 mainshock struck (Moretti et al., 2012). For the 96 earthquakes in the catalog that occurred before the deployment of the temporary network (see Fig. 6), the adopted model is unsatisfactory, even with station corrections, therefore for these events we use the location reported in the ISIDe database (green symbols in Fig. 6; data source: ISIDe).

The entire relocated earthquake catalog was then complemented by the calculation of new M_L values accounting for changes in event location and through the application of station corrections, specifically determined for the study source region. These are especially needed in the study area, because of the soft nature of the soil strongly amplifying ground shaking, thus resulting into an overestimation of the magnitude of smaller events, i.e. those recorded only at close stations, deployed in the Po alluvial plain (Marzorati and Bindi, 2006).

The characteristics of the seven strongest events ($M_L \geq 5.0$; stars in Fig. 6) of the entire seismic sequence are summarized in Table 1. For

each of them, location, M_L values, seismic moment and focal mechanism parameters are reported, if available. Three of these stronger events occurred before the temporary seismic network started operating (green stars in Fig. 6), therefore for them the ISIDe database location is reported (data source: ISIDe). Also two of these events were closely preceded or followed by other earthquakes that hindered the inversion for the TDMT calculation (Scognamiglio et al., 2012; see also http://cnt.rm.ingv.it/tdmt.html), as well as the calculation of focal mechanism from P-wave first-motion polarities, therefore no focal parameters are available for them.

The frequency–magnitude distribution of the relocated earthquake catalog has been then computed following the maximum

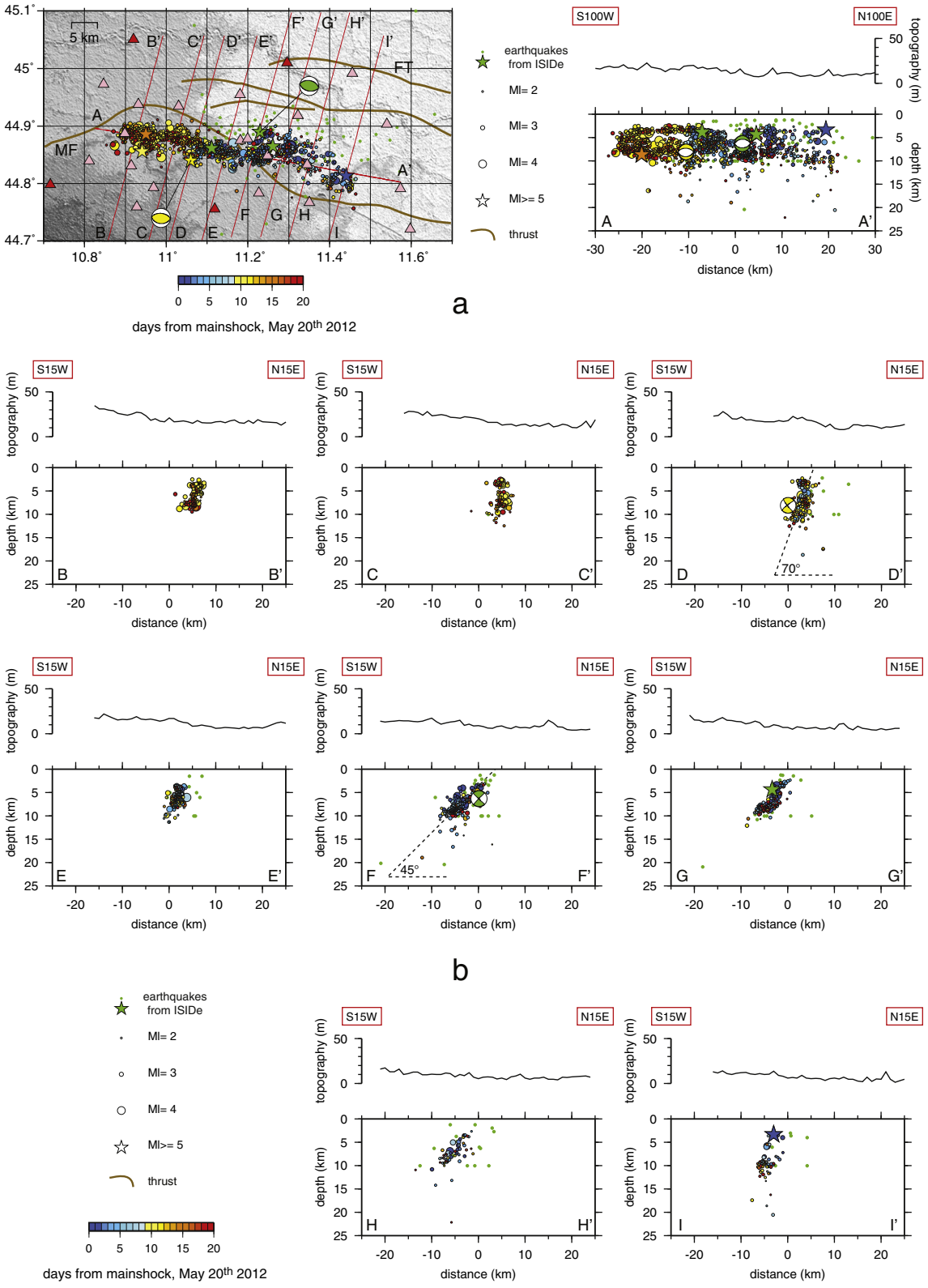

Please cite this article as: Govoni, A., et al., The 2012 Emilia seismic sequence (Northern Italy): Imaging the thrust fault system by accurate aftershock location, Tectonophysics (2014), http://dx.doi.org/10.1016/j.tecto.2014.02.013

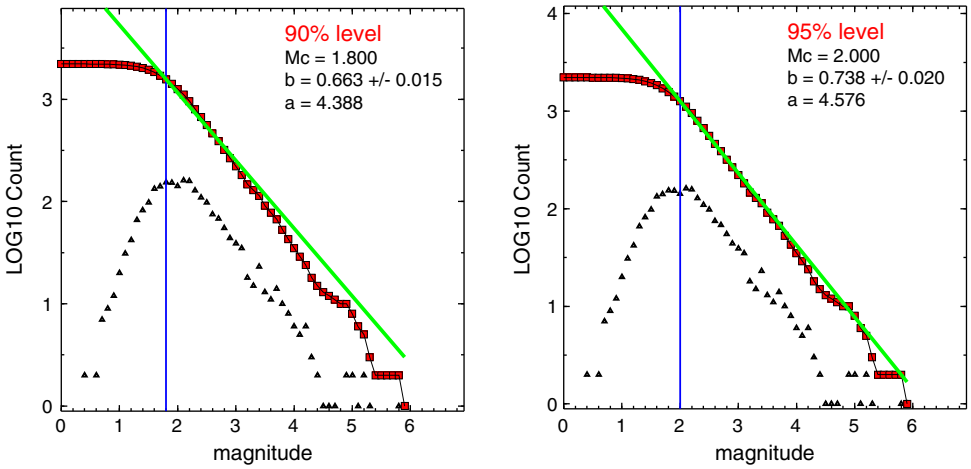

Fig. 7. Frequency–magnitude distributions (FMDs) of the relocated earthquake catalog. The cumulative and non-cumulative numbers of earthquakes are shown by red squares and black triangles, respectively. The green lines represent maximum likelihood fits to the data for magnitudes above the magnitude of completeness at 90% (left panel) and 95% (right panel) levels, respectively (Wiemer and Wyss, 2000), with the blue lines indicating MC: 1.8 for 90% and 2.0 for 95% levels, respectively. (For interpretation of the references to color in this figure legend, the reader is referred to the web version of this article.)

likelihood estimate approach (Aki, 1965). We determine the magnitude of completeness M_C – as well as the complementary seismicity parameter a- and b-values – as the magnitude at which either 90% or 95% of the data (Fig. 7a, b) can be modeled by a power law fit (Wiemer and Wyss, 2000). The computed magnitudes of completeness values are 1.8 and 2.0, at 90% and 95% levels, respectively (Fig. 7, left and right panels). These relatively high thresholds – considering the dense seismic network deployed – are due to the high ambient noise in the area, further amplified at stations by the alluvial nature of soils. Although the fit of the frequency–magnitude distribution (both thresholds) returns quite low b-values (Fig. 7, left and right panels), a discussion on the implication of these values is beyond the scope of the present study, and we leave this issue for further works.

6. Geometry of the fault system and timing of fault segments activation

The aftershock distribution delineates a broad E–W trending, south-dipping structure extended for about 50 km from the central portion of the Ferrara fold-and-thrust system to the frontal thrust of the Mirandola system (Fig. 6, map and cross section AA'). Hypocenters are confined in the upper 12 km depth (Fig. 6). Earthquakes define two separate segments at least, arranged in a left-stepping en-echelon pattern, whose dip changes from steeper to flatter going from west to east (Fig. 6, cross sections going from BB' to II'). From the cross sections drawn in Fig. 6, across the two main shocks we estimate the dip of the western (cross section DD', through the 29th May event) and eastern (cross section FF' through the 20th May event) fault segments to be approximately 70° and 45°, respectively.

The change of dip of the ruptured fault segments from steeper to flatter (between cross sections DD' and EE' in Fig. 6) takes place just at the western edge of the cloud of aftershocks subsequent to the first, M_L 5.9, mainshock, on May 20 (Fig. 8a, map and cross section). At this edge, on May 29, the second, M_L 5.8, major event struck (Fig. 8a). From that moment onward, the barycenter of the whole aftershock sequence shifts toward west, and the vast majority of the earthquakes occur west of the second mainshock hypocenter (Fig. 8b, map and cross section). This observation is corroborated by independent studies carried out on rupture directivity of the two mainshocks. According to Piccinini et al. (Piccinini et al., submitted for publication), in fact, rupture propagates eastward and down-dip for the May 20th and mainly westward for May 29th mainshock. We also observe that in the first nine-day after the 20th May mainshock (Fig. 8a), the relocated seismicity delineate relatively low angle structures (Fig. 6, cross sections going from EE' to II'), while the aftershocks that occurred after the 29th May mainshock, and west of it (Fig. 8b) define high angle fault segments (Fig. 6, cross sections going from BB' to DD'). The close correspondence between structural (Fig. 6) and temporal (Fig. 8) partitioning in the east–west evolution of the seismicity supports the hypothesis that at least two distinct, independent faults, or fault systems, were activated during the Emilia seismic sequence, making room for further investigation on the role of static Coulomb stress redistribution and/or on the possible control of pore fluid pressure diffusion on fault failure (Chiarabba et al., 2009; Malagnini et al., 2012b; Miller et al., 2004).

The different dip of the two main fault segments responsible for the 20th and the 29th May 2012 mainshocks (M_L 5.9 and 5.8, respectively) is not modeled in any of the papers dealing with fault-plane solutions of the Emilia seismic sequence published so far (Cesca et al., 2013; Malagnini et al., 2012a; Pondrelli et al., 2012; Saraò and Peruzza,

Fig. 6. Map (top left) and cross sections through the Emilia seismic sequence, up to 20 June 2012. Earthquakes are sized by magnitude according to the symbols on the right of the map and color-coded by time of occurrence from the first mainshock (May 20th) according to the scale on bottom. To enhance the distinction between western and eastern fault segment seismicity, the color scale spans the first twenty days only; earthquakes that occurred beyond 9th June 2012 are full red colored. The green and yellow beach balls indicate the May 20th and May 29th mainshocks, respectively (solutions are taken from http://cnt.rm.ingv.it/tdmt.html). Stars are the largest events ($M_L \geq 5.0$), including the two mainshocks. Green symbols – circles, stars and beach ball – represent earthquakes whose location has been taken from the ISIDe database (see text for details). Triangles are seismic stations, used to localize earthquakes, belonging to INGV permanent (red triangles) and temporary (pink triangles) seismic networks. Red lines are the traces of the vertical cross-sections, from AA' to II'. Brown curved lines represent the main buried thrusts, the Mirandola Front (MF) and the Ferrara Thrust (FT) (see Fig. 1). Background of the map is a topographic model of Italy with 90 m resolution grid. On the "along-strike" cross section, AA', we project all the events located within 10 km from the vertical plane (i.e. the whole set of analyzed seismicity). Here, the location of the two mainshock is indicated by the respective beach balls. On the cross sections going from BB' to II' we project the earthquakes located within 1.5 km from the vertical planes. The cross sections DD' and FF' are drawn across the 29th and 20th May mainshocks, respectively. Symbols on the cross-sections are the same as in the map view. On each cross section, the topographic profile is also drawn. (For interpretation of the references to color in this figure legend, the reader is referred to the web version of this article.)

Please cite this article as: Govoni, A., et al., The 2012 Emilia seismic sequence (Northern Italy): Imaging the thrust fault system by accurate aftershock location, Tectonophysics (2014), http://dx.doi.org/10.1016/j.tecto.2014.02.013

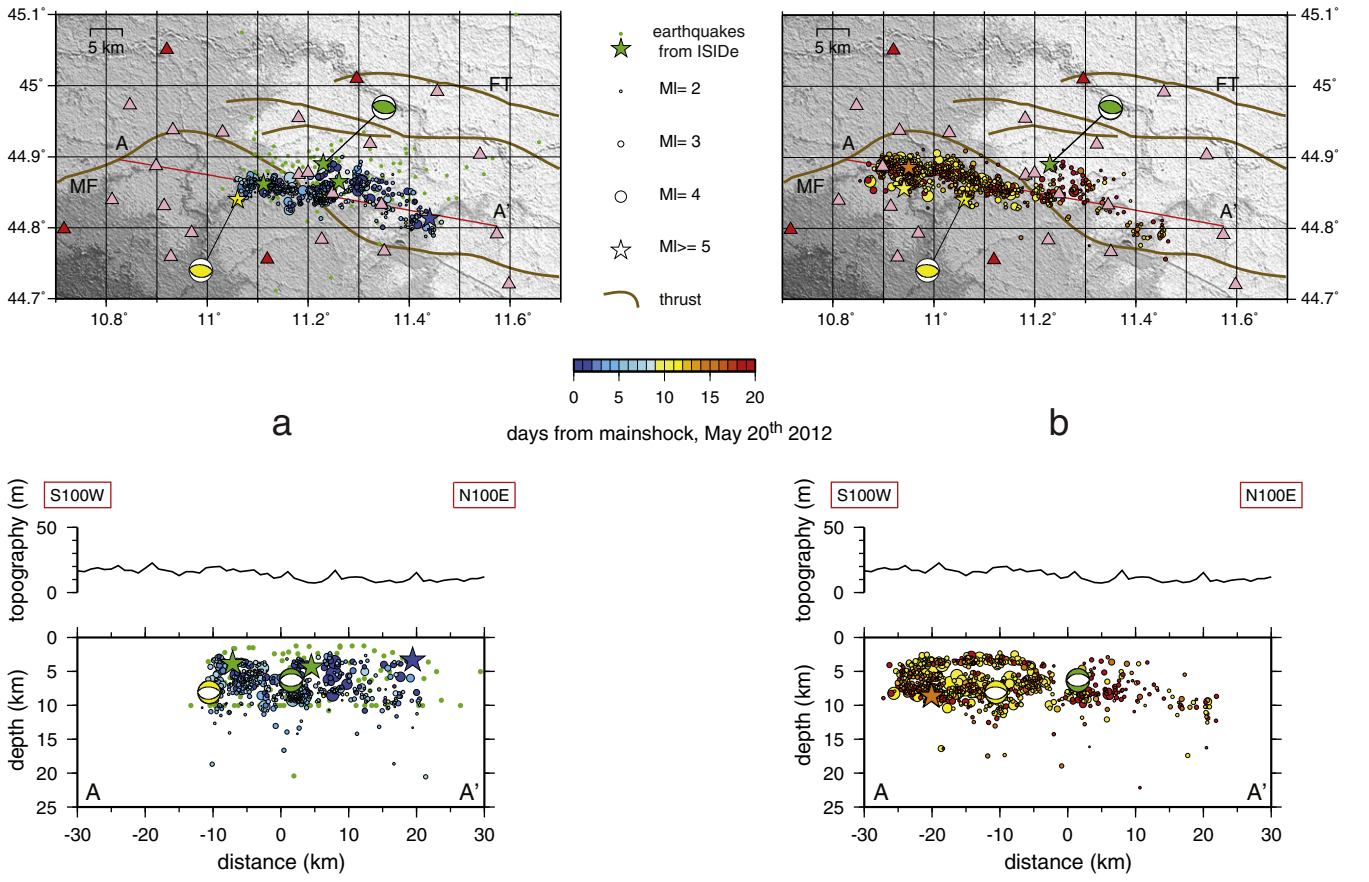

Fig. 8. (a) Map and "along-strike" cross section, AA', through the Emilia seismic sequence, in the time span from the 20th May, M_L 5.9, first mainshock (green beach ball) to the 29th May, M_L 5.8, second mainshock (yellow beach ball). (b) Map and "along-strike" cross section, AA', through the Emilia seismic sequence, in the time span from the 29th May, M_L 5.8, second mainshock (yellow beach ball) to the 20th June. On both panel a and b AA' cross sections, all the events located within 10 km from the vertical plane are projected. There, the location of the two mainshock is indicated by the respective beach balls. On both panel a and b maps and cross sections, symbols and color-coding are the same as in Fig. 6. Background of the maps is a topographic model of Italy with 90 m resolution grid. (For interpretation of the references to color in this figure legend, the reader is referred to the web version of this article.)

2012; Scognamiglio et al., 2012). All these authors indeed obtain very similar solutions for the two mainshocks, displaying low dip angles for the south dipping planes. The discrepancy observed between the relocated aftershock alignments on the westernmost fault segment and fault-plane solutions computed by the above authors for the 29th May, M_L 5.8, mainshock (Fig. 6, cross section DD') poses therefore some puzzling questions on the actual geometry of the fault system. One possible explanation, as suggested by Cesca et al. (2013), is that the 29th May mainshock struck at the deeper, flatter portion of a fault segment of listric geometry, with most of the aftershocks shown in Fig. 6 (cross sections going from BB' to DD') occurring on the shallow, steeper part.

The different dip of the two fault segments suggested by relocated aftershocks is also coherent with updated source models of the 20th and the 29th May shocks obtained by ground deformation InSAR data (Tizzani et al., 2013). Advanced modeling based on a finite-element structural–mechanical method confirms the activation of a single, low-angle, fault segment for the 20th May, M_L 5.9, shock. Conversely, the best-fit source model for the 29th May, M_L 5.8, event includes the involvement of three fault-segments describing an overall listric geometry, with the steeper part that dips about 65° between 5 and 8 km depths (see Fig. 3h in Tizzani et al. (2013)).

In order to further assess this interesting point, we analyze the statistical distribution of P and T axis geometry retrieved from about 800 focal mechanisms computed from the P-wave first-motion polarity data using the FPFIT algorithm (Reasenberg and Oppenheimer, 1985). We select all focal solutions with rake values ranging from 60 to 120 – i.e. using the definition of reverse fault type in terms of rake angle given in Boore and Atkinson (2007) – and assign each of them to the western or eastern fault segment depending on the longitude of the events (Lon < 11.15 to western segment; Lon > 11.15 to eastern segment). We then compute P and T axes for focal mechanisms of events on the two fault segments. The statistical distributions of P- and T-axis plunges are shown in Fig. 9. On the eastern segment (Fig. 9, bottom panels) the P-axis plunges are generally lower then 20°, being the 0°–10° class the most populated, while on the western segment P-axis plunges tend to be greater than 20°, with a prevalence of values in the 20°–30° class (Fig. 9, top panels). Also T-axis plunges vary, being on the eastern segment generally steeper than on the western one. P- and T-axis plunges computed for a theoretical reverse fault (rake = 90) with a 70° dipping-plane (as for the western segment, Fig. 6, cross section DD') are 25° and 65°, respectively, in agreement with the statistic distribution shown in Fig. 9 (top panels). Whereas, for a classical reverse fault with a 45° dipping-plane (simulating the eastern segment, Fig. 6, cross section FF') plunges are 0° and 90°, for P and T axes, respectively. Result of this simple calculation can further corroborate the hypothesis that the 29th May, M_L 5.8, shock nucleated at the base of a seismogenic structure whose geometry varies with depth: being flatter in its deeper part, thus justifying the low dip angles modeled in fault-plane solutions (Cesca et al., 2013; Malagnini et al., 2012a; Pondrelli et al., 2012; Saraò and Peruzza, 2012; Scognamiglio et al., 2012), and becoming steeper in its shallow portion, where most of the aftershocks occurred, thus accounting for the observed statistical distribution of P- and T-axis plunges there.

Please cite this article as: Govoni, A., et al., The 2012 Emilia seismic sequence (Northern Italy): Imaging the thrust fault system by accurate aftershock location, Tectonophysics (2014), http://dx.doi.org/10.1016/j.tecto.2014.02.013

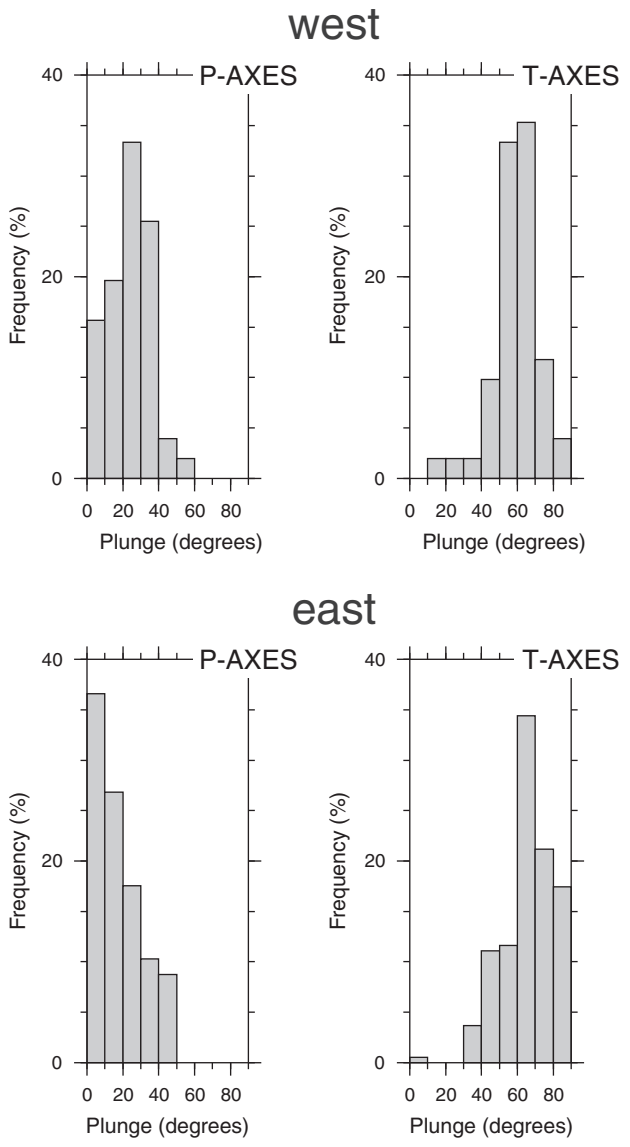

Fig. 9. Statistical distribution of P and T axis plunges for earthquakes that occurred on the western (top panels) and eastern (bottom panels) fault segment — west or east of Lon 11.15, respectively. The P and T axes were retrieved from about 800 focal mechanisms computed from the P-wave first-motion polarity data. The two sets show a different distribution of the P and T axis plunges, consistent with the different dip of the western and eastern fault segments imaged by the relocated aftershock hypocenters.

7. Seismotectonic interpretation

In order to provide a seismotectonic interpretation of the seismic sequence and a first-order earthquake–fault association, we compared aftershock locations to the geometry of the fold-and-thrust belt. The aftershock region is crossed by two published NNE–SSW striking structural profiles (Fig. 10a). The eastern one (Carminati et al., 2010) extends from the central, WNW–ESE trending, portion of the Ferrara fold-and-thrust system to the eastern flank of the Mirandola system, across the aftershock volume mainly related to the 20th May mainshock. The western profile (Boccaletti et al., 2004) crosses the W–E trending frontal ramp of the Mirandola system, across the western portion of the aftershock region illuminated after the 29th May mainshock. Both sections are featured upon seismic reflection data and constrained by deep oil wells. Due to the presence of not-cylindrical fold-and-thrust structures (Fig. 10a), we project exclusively nearby aftershocks located within 1.5 km from the section, complemented by the two mainshocks projected according to published fault-plane solutions (Scognamiglio et al., 2012).

As shown in the structural map (Fig. 10a) and in the eastern geological section (MM' in Fig. 10c), the Ferrara system is articulated in three main thrust-fold structures (Carminati et al., 2010). Aftershocks concentrate within the Mesozoic–Tertiary carbonates around the innermost and intermediate thrust faults of the Ferrara system. Hypocentral distribution envisages three main SW-dipping alignments. Based on the thrust geometries, and given the uncertainty in the interpretation and depth conversion of the deep reflectors, we can hypothesize the following earthquake–fault associations. A shallow alignment, between 2 and 4 km depths, may be related to the upper portion of the innermost thrust. Between 5 and 7 km, aftershocks cluster in correspondence of the basal portion of the intermediate thrust. A deeper, low-angle alignment is located in the footwall of the intermediate thrust, around 8–9 km depth. This cluster occurs at the base of the Mesozoic units and may be related to a low-angle basal detachment connecting up with the outermost front. Even if hypocenter location of the 20th May mainshock is affected by a larger uncertainty and falls 5 km to the west of the section (Fig. 10a), the map and section views strongly support that this earthquake activated the intermediate thrust of the Ferrara system (Fig. 10c). This is also suggested by the overall consistency among the thrust geometry (strike, length, dip), focal solution of the mainshock and aftershock distribution during the first nine days of the sequence (Fig. 10a). An association to the innermost thrust, as proposed by Tizzani et al. (2013), is unlike because this would imply a very large hypocentral mislocation for the 20th May mainshock, in the order of 6–7 km horizontally.

Along the western geological section (LL' in Fig. 10a) the earthquake–fault association is complicated by the lack of deep seismic information in the footwall side of the Mirandola frontal ramp (Fig. 10b) (Boccaletti et al., 2004). Aftershocks are confined inside the Mesozoic carbonate units and occur both in the hangingwall- and footwall side of the Mirandola frontal thrust, as drawn by Boccaletti et al. (2004). In the hangingwall, aftershocks align around 4 km depth. Conversely, in the footwall, aftershock distribution elongate from 5 to 10 km depth defining a main steep dipping structure. Differently from the eastern profile, we do not find a clear association between known fault geometries and aftershock distribution. At a first glance, location and focal solution of the 29th May mainshock seem compatible with the activation of the basal thrust of the Mirandola system (Fig. 10b), as suggested by most authors (Ventura and Di Giovanbattista, 2013, among others). However, the projection of the mainshock hypocenter on the geological section (MM', Fig. 10b) does not necessarily fit the drawn basal thrust, due to the bent geometry of the Mirandola structures and to the location of this event 7 km to the east of the section (see Fig. 10a). Hence, we cannot rule out the alternative interpretation of Lavecchia et al. (2012) that associated the 29th May mainshock to the westernmost and innermost thrust of the Ferrara system, recognized a few kilometers northward (Fig. 10a). Whatever is the seismotectonic interpretation, we remark that the western section documents the occurrence of numerous aftershocks of the 29th May mainshock, including one M_L 5.3 event, in the footwall side of the Mirandola frontal thrust, activating high-angle deep fault segments in a more external position. Such faults could be ascribed to the westernmost fold–thrust structure of the Ferrara system (Fig. 10a). This finding would suggest a reconsideration of the deep geometry of the outer thrust reported in section by Boccaletti et al. (2004).

8. Discussion

Throughout the May–June 2012, Emilia seismic sequence, seismicity develops inside the Meso-Cenozoic sedimentary cover on segmented ramps bottoming on a regional decollement, that is inferred at depth of about 10 km, according to Scrocca et al. (2007). While the steeper western fault segment ruptured on 29 May likely corresponds to the

Please cite this article as: Govoni, A., et al., The 2012 Emilia seismic sequence (Northern Italy): Imaging the thrust fault system by accurate aftershock location, Tectonophysics (2014), http://dx.doi.org/10.1016/j.tecto.2014.02.013

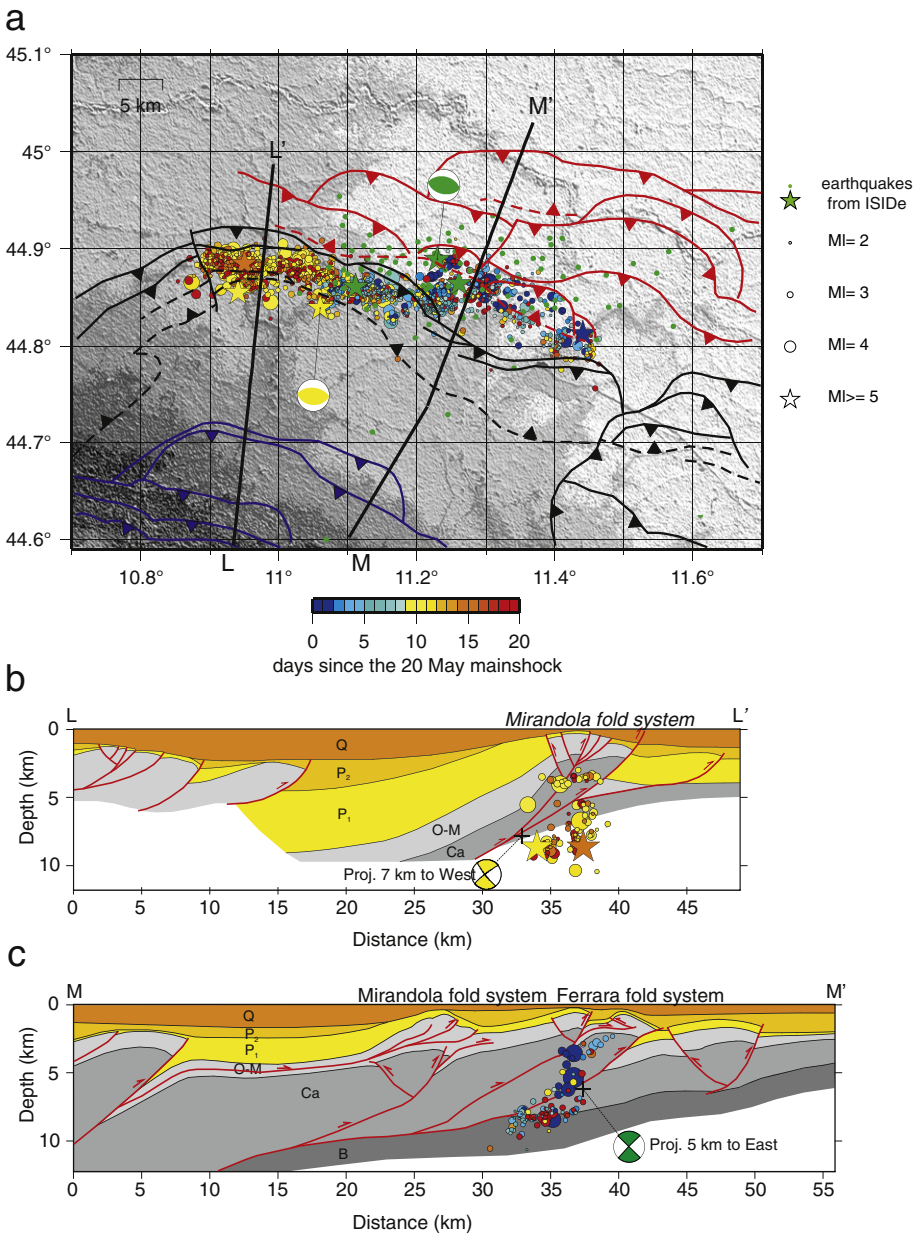

Fig. 10. (a) Map of the spatio-temporal distribution of aftershocks compared to the main thrusts in the Mesozoic–Early Tertiary carbonates. Background, symbols and color-coding for seismicity are the same as in Fig. 6. Thrust and back-thrust of the Ferrara (red), Mirandola (black), and Apenninic (blue) systems are shown with continuous and dashed lines, respectively. Focal solutions of the 20th and 29th May mainshocks are plotted in green and yellow, respectively. Thrust geometries are modified after Bigi et al. (1991) and Boccaletti et al. (2004). (b) Geological section across the frontal ramp of Mirandola fold-and-trust system (modified after Boccaletti et al., 2004) and aftershocks distribution for events located within 1.5 km from the trace of the section. Focal solution and hypocenter of the 29th May mainshock are also shown. (c) Geological section across the Ferrara fold-and-trust system and the eastern flank of the Mirandola system (modified after Carminati et al., 2010) based on the interpretation of the composite seismic profile App-Orient-1 (available from the ViDEPI Project at: http://unmig.sviluppoeconomico.gov.it/videpi/). Aftershocks are located within 1.5 km from the trace of the section. Focal solution and hypocenter of the 20th May mainshock are also shown. Legend: Q — continental and marine Quaternary deposits, P_2 — marine terrigenous deposits (upper-middle Pliocene), P_1 — evaporitic and terrigenous deposits (late Miocene–lower Pliocene), O–M — marly calcareous and terrigeneous deposits (Oligocene–Miocene), Ca — shallow to deep-water carbonates (Mesozoic–Eocene), B — Paleozoic basement.

Mirandola frontal thrust, the flatter eastern segment, responsible for the 20th May mainshock, matches the intermediate thrust of the Ferrara system (Fig. 10a, c), but probably not the outermost one (Fig. 10a, c). Also, aftershock locations and subsurface data suggest the activation of secondary fault segments both in the footwall- and hanging-wall sides of the main thrusts related to the mainshocks. Hence, aftershock pattern mirrors the overall, complex architecture of the Ferrara arc.

During the first 15 days, the seismic sequence shows a very clear progressive activation of adjacent faults or fault segments. Seismicity started on the eastern segment (deep blue colors in Figs. 6 and 8), but rightly after the May 20th mainshock propagated to the west close to the area ruptured during the second mainshock on May 29th (from lighter blue to yellow colors in Figs. 6 and 8). After this second shock, seismicity further propagated westward (from yellow to red colors in Figs. 6 and 8), in an area later struck by two more $M_L \geq 5.0$ events, one on May 29th and the last one on June 3rd (see Table 1). As for other seismic sequence in the Apennines, the involvement of fluids hosted in the folded sedimentary successions could have played a role in modulating the seismicity during the sequence (Calderoni et al., 2009; Malagnini et al., 2012b; Miller et al., 2004; Ventura and Di Giovambattista, 2013).

Soon after the second mainshock, a great concern was posed by the possibility that the seismicity could further propagate on adjacent

portions of the thrust system. From June 2012, seismicity remained confined within the already ruptured portions of the fault system.

The western termination of seismicity (Fig. 2) coincides with the frontal ramp of the Mirandola system and seems to follow a NNW–SSE trending, left-lateral transcurrent structure that dissects the arc (Fig. 10a). Along the western flank of the Mirandola arc, the closest seismicity corresponds to the 1996, M_W 5.4 Reggio Emilia sequence that occurred about 30 km to west of the 2012 Emilia sequence (Fig. 1a) (Ciaccio and Chiarabba, 2002; Selvaggi et al., 2001).

In the eastern part of the Ferrara fault system, the situation is different. During the entire sequence, seismicity did not propagate eastward of the main first ruptured fault. In this area, instrumental seismicity of past 30 years was very low (Chiarabba et al., 2005), while a severe and prolonged seismic sequence occurred in 1570 (data source: CPTI11 after Rovida et al. (2011)). The structure of the fault system also changes at depth (Toscani et al., 2009), and the relation between active faults and minor thrust splays is less documented. Although, the large previous series of earthquakes occurred almost 450 years ago, the small compressional strain rate of about 1 mm/yr (Devoti et al., 2011) might indicate a maximum slip deficit of about 0.5 m, if the fault system is entirely locked. This value is consistent with the average slip value on the activated faults inferred by Pezzo et al. (2013) through geodetic data modeling. The available historical and instrumental data do not allow addressing more deeply the question on how far the eastern part of the fault system is prone to relevant earthquakes.

9. Conclusions

Mainshocks and aftershocks of the 2012 Emilia seismic sequence reveal the activation of a complex thrust fault system composed by at least two main distinct faults, belonging to the Ferrara and Mirandola arcs. The two structures have different dip and correspond to two faults ramping from a deep decollement located at about 10-km depth. Relocated aftershocks suggest that the 29th May, M_L 5.8, event occurred on a thrust fault whose geometry varies with depth, becoming steeper in its upper portion. This result is consistent with source models obtained by advanced modeling of ground deformation InSAR data (Tizzani et al., 2013) and represents the first seismological evidence of a source complexity that was not captured by previous fault-plane solutions of the 29th May, M_L 5.8, shock (see among the others Scognamiglio et al. (2012)). Also, aftershock distribution documents the activation of steep dipping fault segments in the footwall side of the Mirandola frontal thrust.

The whole Apennine external arc is accommodating a compressional rate of a few mm/yr revealed by geodetic data, and the front, although regionally branched in three main arcs, is active along its total length.

The seismic sequence, similar to other sequences occurred in recent years and historically in the Apennines, is composed by multiple shocks that correspond to the rupture of contiguous fault segments and presents a clear migration. Seismicity first developed on the Ferrara outer system, and rapidly propagated to the west toward the fault system on which the May 29 shock originated, i.e. the Mirandola front, and finally moved further west at the closure of the Ferrara arc, where two more $M_L \geq 5.0$ events occurred in the subsequent hours/days.

This study paves the way for future investigation, which should address the seismic hazard close to the eastern termination of the activated area.

Aknowledgements

The authors would like to thank the editor and two reviewers for their suggestions and valuable comments that greatly improved the manuscript.This paper would not have been possible without the support of many people. The authors wish to thank all the staff working for the mobile networks in Rome, Ancona, Bologna, Milano and Grottaminarda who deployed and maintained the seismic network during the sequence. Special thanks are also due to Valentino Lauciani, Andrea Bono, Stefano Pintore, Salvatore Mazza and all the staff working at the INGV EIDA data-bank that helped to qualify and manage such a large data set. NPA research is supported by Science Foundation Ireland & the Marie-Curie Action COFUND under Grant Number 11/SIRG/E2174.

Appendix A. Supplementary data

Supplementary data associated with this article can be found in the online version, at http://dx.doi.org/10.1016/j.tecto.2014.02.013. These data include Google map of the most important areas described in this article.

References

Aki, K., 1965. Maximum likelihood estimate of b in the formula log N = a − bM and its confidence limits. Bull. Earthq. Res. Inst., Univ. Tokyo 43 (2), 237–239.

Artemieva, I.M., 2002. Continental Crust. in Encyclopedia of Life Support Systems (EOLSS): Developed under the Auspices of the UNESCO. EOLSS Publishers, Oxford, UK. Chapter 6.16.3.1 (http://www.eolss.net).

Bigi, S., Cosentino, D., Parotto, M., Sartori, R. and Scandone P., 1991. Structural model of Italy. Scale 1:500.000. C.N.R., Progetto Finalizzato Geodinamica, Selca, Florence (Italy).

Boccaletti, M., Bonini, M., Corti, G., Gasperini, P., Martelli, L., Piccardi, L., Tanini, C., Vannucci, G., 2004. Carta simotettonica della regione Emilia Romagna, 1:250.000 e note illustrative, SELCA Editore, Firenze.

Boccaletti, M., Corti, G., Martelli, L., 2011. Recent and active tectonics of the external zone of the Northern Apennines (Italy). Int. J. Earth Sci. 100 (6), 1331–1348. http://dx.doi.org/10.1007/s00531-010-0545-y.

Boore, D.M., Atkinson, G.M., 2007. Boore–Atkinson NGA ground motion relations for the geometric mean horizontal component of peak and spectral ground motion parameters. PEER Report 2007/01Pacific Earthquake Engineering Research Center College of Engineering University of California, Berkeley (110 pp.).

Bordoni, P., Azzara, R.M., Cara, F., Cogliano, R., Cultrera, G., Di Giulio, G., Fodarella, A., Milana, G., Pucillo, S., Riccio, G., Rovelli, A., Augliera, P., Luzi, L., Lovati, S., Massa, M., Pacor, F., Puglia, R., Ameri, G., 2012. Preliminary results from EMERSITO, a rapid response network for site-effect studies. Ann. Geophys. 55 (4), 599–607. http://dx.doi.org/10.4401/ag-6153.

Burrato, P., Ciucci, F., Valensise, G., 2003. An inventory of river anomalies in the Po Plain, Northern Italy: evidence for active blind thrust faulting. Ann. Geophys. 46 (5), 865–882. http://dx.doi.org/10.4401/ag-3459.

Calderoni, G., Di Giovambattista, R., Burrato, P., Ventura, G., 2009. A seismic sequence from northern Apennines (Italy) provides new insight on the role of fluids in the active tectonics of accretionary wedges. Earth Planet. Sci. Lett. 281 (1–2), 99–109. http://dx.doi.org/10.1016/j.epsl.2009.02.015.

Carminati, E., Scrocca, D., Doglioni, C., 2010. Compaction-induced stress variations with depth in an active anticline: Northern Apennines, Italy. J. Geophys. Res. 115 (B02401). http://dx.doi.org/10.1029/2009JB006395.

Castello, B., Selvaggi, G., Chiarabba, C., Amato, A., 2006. CSI Catalogo della sismicità italiana 1981–2002, version 1.1. INGV-CNT, Roma. available at: http://www.ingv.it/CSI/.

Cesca, S., Braun, T., Maccaferri, F., Passarelli, L., Rivalta, E., Dahm, T., 2013. Source modelling of the M5–6 Emilia–Romagna, Italy, earthquakes (2012 May 20–29). Geophys. J. Int. 193 (3), 1658–1672. http://dx.doi.org/10.1093/gji/ggt069.

Chatelain, J.L., 1978. Etude fine de la sismicité en zone de collision continentale au moyen d'un réseau de stations portables: la région Hindu-Kush Pamir. Thèse de doctorat de 3ème cycle Université scientifique et médicale de Grenoble (219 pp.).

Chiarabba, C., Jovane, L., Di Stefano, R., 2005. A new view of Italian seismicity using 20 years of instrumental recordings. Tectonophysics 395, 251–268. http://dx.doi.org/10.1016/j.tecto.2004.09.013.

Chiarabba, C., De Gori, P., Boschi, E., 2009. Pore pressure migration along a normal fault system resolved by time-repeated seismic tomography. Geology 37 (12), 67–70.

Ciaccio, M.G., Chiarabba, C., 2002. Tomographic models and seismotectonics of the Reggio Emilia region, Italy. Tectonophysics 344 (1–2), 261–276. http://dx.doi.org/10.1016/S0040-1951(01)00275-X.

Ciccotti, M., Mulargia, F., 2004. Differences between static and dynamic elastic moduli of a typical seismogenic rock. Geophys. J. Int. 157, 474–477. http://dx.doi.org/10.1111/j.1365-246X.2004.02213.x.

Devoti, R., Esposito, A., Pietrantonio, G., Pisani, A.R., Riguzzi, F., 2011. Evidence of large scale deformation patterns from GPS data in the Italian subduction boundary. Earth Planet. Sci. Lett. 311 (3–4), 230–241. http://dx.doi.org/10.1016/j.epsl.2011.09.034.

Emergeo Working Group, 2013. Liquefaction phenomena associated with the Emilia earthquake sequence of May–June 2012 (Northern Italy). Nat. Hazards Earth Syst. Sci. 13, 935–947. http://dx.doi.org/10.5194/nhess-13-935-2013.

Enescu, B., Mori, J., Miyazawa, M., 2007. Quantifying early after-shock activity of the 2004 mid-Niigata Prefecture earthquake (M_W 6.6). J. Geophys. Res. 112 (B04310). http://dx.doi.org/10.1029/2006JB004629.

Fantoni, R., Franciosi, R., 2010. Tectono-sedimentary setting of the Po Plain and Adriatic foreland. Rend. Fis. Acc. Lincei 21 (Suppl. 1), 197–209. http://dx.doi.org/10.1007/s12210-010-0102-4.

Please cite this article as: Govoni, A., et al., The 2012 Emilia seismic sequence (Northern Italy): Imaging the thrust fault system by accurate aftershock location, Tectonophysics (2014), http://dx.doi.org/10.1016/j.tecto.2014.02.013

ISIDe Working Group, 2010. Italian Seismological Instrumental and parametric Database. http://iside.rm.ingv.it.

Kissling, E., Ellsworth, W.L., Eberhart-Phillips, D., Kradolfer, U., 1994. Initial reference models in seismic tomography. J. Geophys. Res. 99 (B10), 19635–19646.

Klein, F.W., 2002. User's guide to HYPOINVERSE-2000: a Fortran program to solve for earthquake locations and magnitudes. USGS Open File Report 02-171, Version 1.0 1–123.

Lahr, J.C., 1989. Hypoellipse/version 2.0: a computer program for determining local earthquake hypocentral parameters, magnitude and first motion pattern. U.S. Geological Survey Open-file Report 89-116 (92 pp.).

Lavecchia, G., De Nardis, R., Cirillo, D., Brozzetti, F., Boncio, P., 2012. The May–June 2012 Ferrara arc earthquakes (northern Italy): structural control of the spatial evolution of the seismic sequence and of the surface pattern of coseismic fractures. Ann. Geophys. 55, 4. http://dx.doi.org/10.4401/ag-6173.

Malagnini, L., Herrmann, R.B., Munafò, I., Buttinelli, M., Anselmi, M., Akinci, A., Boschi, E., 2012a. The 2012 Ferrara seismic sequence: regional crustal structure, earthquake sources, and seismic hazard. Geophys. Res. Lett. 39 (L19302). http://dx.doi.org/10.1029/2012GL053214.

Malagnini, L., Lucente, F.P., De Gori, P., Akinci, A., Munafo', I., 2012b. Control of pore fluid pressure diffusion on fault failure mode: insights from the 2009 L'Aquila seismic sequence. J. Geophys. Res. 117 (B05302). http://dx.doi.org/10.1029/2011JB008911.

Margheriti, L., Azzara, R., Cocco, M., Delladio, A., Nardi, A., 2000. Analyses of borehole broadband recordings: test site in the Po basin, Northern Italy. Bull. Seismol. Soc. Am. 90, 1454–1463. http://dx.doi.org/10.1785/0119990061.

Marzorati, S., Bindi, D., 2006. Ambient noise levels in north central Italy. Geochem. Geophys. Geosyst. 7 (9). http://dx.doi.org/10.1029/2006GC001256.

Miller, S.A., Collettini, C., Chiaraluce, L., Cocco, M., Barchi, M.R., Kaus, B., 2004. Aftershocks driven by a high pressure CO_2 source at depth. Nature 27, 724–727.

Montone, P., Mariucci, M.T., Pierdominici, S., 2012. The Italian present-day stress map. Geophys. J. Int. 189 (2), 705–716. http://dx.doi.org/10.1111/j.1365-246X.2012.05391.x.

Moretti, M., et al., 2012. Rapid response to the earthquake emergency of May 2012 in the Po Plain, northern Italy. Ann. Geophys. 55 (4), 583–590. http://dx.doi.org/10.4401/ag-6152.

MPS Working Group, 2004. Redazione della mappa di pericolosità sismica prevista dall'Ordinanza PCM 3274 del 20 Marzo 2003. Rapporto Conclusivo per il Dipartimento della Protezione Civile, INGV, Milano—Roma, April 2004 (65 pp., including 5 appendixes. http://zonesismiche.mi.ingv.it).

Papathanassiou, G., Caputo, R., Rapti-Caputo, D., 2012. Liquefaction phenomena along the paleo-Reno River caused by the May 20, 2012, Emilia (northern Italy) earthquake. Ann. Geophys. 55 (4), 735–742. http://dx.doi.org/10.4401/ag-6147.

Pezzo, G., Merryman, J.P., Tolomei, C., Salvi, S., Atzori, S., Antonioli, A., Trasatti, E., Novali, F., Serpelloni, E., Candela, L., Giuliani, R., 2013. Coseismic deformation and source modeling of the May 2012 Emilia (Northern Italy) earthquakes. Seismol. Res. Lett. 84 (4), 645–655. http://dx.doi.org/10.1785/0220120171.

Piccinini, D., Pino, N.A., Saccorotti, G., 2014. Rupture propagation affecting damage distribution and ground effects: evidences from the Emilia 2012, Italy, mainshocks. J. Geophys. Res. (submitted for publication).

Picotti, V., Pazzaglia, F.J., 2008. A new active tectonic model for the construction of the Northern Apennines mountain front near Bologna (Italy). J. Geophys. Res. 113, B08412. http://dx.doi.org/10.1029/2007JB005307.

Pondrelli, S., Salimbeni, S., Ekström, G., Morelli, A., Gasperini, P., Vannucci, G., 2006. The Italian CMT dataset from 1977 to the present. Phys. Earth Planet. Inter. 159 (3–4), 286–303. http://dx.doi.org/10.1016/j.pepi.2006.07.008.

Pondrelli, S., Salimbeni, S., Perfetti, P., Danecek, P., 2012. Quick regional centroid moment tensor solutions for the Emilia 2012 (northern Italy) seismic sequence. Ann. Geophys. 55 (4), 599–607. http://dx.doi.org/10.4401/ag-6146.

Reasenberg, P.A., Oppenheimer, D., 1985. FPFIT, FPPLOT, and FPPAGE: FORTRAN computer programs for calculating and displaying fault plane solutions. U.S. Geological Survey Open File Report 85-739 (109 pp.).

Reutter, K.J., Giese, P., Closs, H., 1980. Lithospheric split in the descending plate: observations from the Northern Apennines. Tectonophysics 64 (1–2), T1–T9. http://dx.doi.org/10.1016/0040-1951(80)90254-1.

Rovida, A., Camassi, R., Gasperini, P., Stucchi, M. (Eds.), 2011. CPTI11, the 2011 Version of the Parametric Catalogue of Italian Earthquakes (Milano, Bologna, http://emidius.mi.ingv.it/CPTI. http://dx.doi.org/10.6092/INGV.IT-CPTI11).

Saraò, A., Peruzza, L., 2012. Fault-plane solutions from moment-tensor inversion and preliminary Coulomb stress analysis for the Emilia Plain. Ann. Geophys. 55 (4), 647–654. http://dx.doi.org/10.4401/ag-6134.

Scognamiglio, L., Margheriti, L., Mele, F.M., Tinti, E., Bono, A., De Gori, P., Lauciani, V., Lucente, F.P., Mandiello, A.G., Marcocci, C., Mazza, S., Pintore, S., Quintiliani, M., 2012. The 2012 Pianura Padana Emiliana seismic sequence: locations, moment tensors and magnitudes. Ann. Geophys. 55 (4), 549–559. http://dx.doi.org/10.4401/ag-6159.

Scrocca, D., Carminati, E., Doglioni, C., Marcantoni, D., 2007. Slab retreat and active shortening along the central-northern Apennines. In: Lacombe, O., et al. (Eds.), Thrust Belts and Foreland Basins: From Fold Kinematics to Hydrocarbon Systems, Frontiers in Earth Sciences. Springer, Berlin, pp. 471–487.

Selvaggi, G., Ferulano, F., Di Bona, M., Frepoli, A., Azzara, R., Basili, A., Chiarabba, C., Ciaccio, M.G., Di Luccio, F., Lucente, F.P., Margheriti, L., Nostro, C., 2001. The MW 5.4 Reggio Emilia 1996 earthquake: active compressional tectonics in the Po Plain, Italy. Geophys. J. Int. 144 (1), 1–13. http://dx.doi.org/10.1046/j.0956-540X.2000.01255.x.

Serpelloni, E., Anzidei, M., Baldi, P., Casula, G., Galvani, A., 2005. Crustal velocity and strain-rate fields in Italy and surrounding regions: new results from the analysis of permanent and non-permanent GPS networks. Geophys. J. Int. 161 (3), 861–880. http://dx.doi.org/10.1111/j.1365-246X.2005.02618.x.

Tertulliani, A., Arcoraci, L., Berardi, M., Bernardini, F., Brizuela, B., Castellano, C., Del Mese, S., Ercolani, E., Graziani, L., Maramai, A., Rossi, A., Sbarra, M., Vecchi, M., 2012. The Emilia 2012 sequence: a macroseismic survey. Ann. Geophys. 55 (4), 679–687. http://dx.doi.org/10.4401/ag-6140.

Tizzani, P., Castaldo, R., Solaro, G., Pepe, S., Bonano, M., Casu, F., Manunta, M., Manzo, M., Pepe, A., Samsonov, S., Lanari, R., Sansosti, E., 2013. New insights into the 2012 Emilia (Italy) seismic sequence through advanced numerical modeling of ground deformation InSAR measurements. Geophys. Res. Lett. 40, 1–7. http://dx.doi.org/10.1002/grl.50290.

Toscani, G., Burrato, P., Di Bucci, D., Seno, S., Valensise, G., 2009. Plio-Quaternary tectonic evolution of the northern Apennines thrust fronts (Bologna–Ferrara section, Italy): seismotectonic implications. Bollettino della Società Geologica Italiana e del Servizio Geologico d'Italia (Italian Journal of Geosciences), 128 605–613. http://dx.doi.org/10.3301/IJG.2009.128.2.605.

Trippetta, F., Collettini, C., Meredith, P.G., Vinciguerra, S., 2013. Evolution of the elastic moduli of seismogenic Triassic evaporites subjected to cyclic stressing. Tectonophysics 592, 67–79. http://dx.doi.org/10.1016/j.tecto.2013.02.011.

Valoroso, L., Improta, L., De Gori, P., Chiarabba, C., 2011. Upper crustal structure, seismicity and pore pressure variations in an extensional seismic belt through 3D and 4D Vp and Vp/Vs models: the example of the Val d'Agri area (Southern Italy). J. Geophys. Res. 116, B07303. http://dx.doi.org/10.1029/2010JB007661.

Ventura, G., Di Giovambattista, R., 2013. Fluid pressure, stress field and propagation style of coalescing thrusts from the analysis of the 20 May 2012 M_L 5.9 Emilia earthquake (Northern Apennines, Italy). Terra Nova 25, 72–78. http://dx.doi.org/10.1111/ter.12007.

Wadati, K., 1933. On the travel time of earthquake waves. Part II. Geophys. Mag. 7, 101–111.

Wiemer, S., Wyss, M., 2000. Minimum magnitude of completeness in earthquake catalogs: examples from Alaska, the western United States, and Japan. Bull. Seismol. Soc. Am. 90 (4), 859–869. http://dx.doi.org/10.1785/0119990114.

Please cite this article as: Govoni, A., et al., The 2012 Emilia seismic sequence (Northern Italy): Imaging the thrust fault system by accurate aftershock location, Tectonophysics (2014), http://dx.doi.org/10.1016/j.tecto.2014.02.013